Experimental investigation on a passive self-tuning vibration neutraliser for two distinct frequencies

Journal of Physics: Conference Series **2647** (2024) 032006 doi:10.1088/1742-6596/2647/3/032006

Experimental investigation on a passive self-tuning vibration neutraliser for two distinct frequencies

G F Nehemy[1], E Rustighi[2], P J P Gonçalves[1] and M J Brennan[1]
[1]State University of São Paulo (UNESP), School of Engineering, Bauru, Brazil
[2]Industrial Engineering Department, University of Trento, Povo, Trento, Italy
E-mail: gabriella.nehemy@unesp.br, emiliano.rustighi@unitn.it, paulo.paupitz@unesp.br, mjbrennan0@btinternet.com

Abstract. Tuned vibration neutralisers are used to suppress the vibration of a host structure subjected to external harmonic forces. Although they are analogous to tuned vibration absorbers, the primary difference is that while absorbers are usually designed with optimum damping to attenuate vibration in a frequency range around a resonance, neutralisers are designed with relatively low damping to act as a mechanical notch-filter. The narrow band frequency in which the conventional neutralisers are effective, and the mistuning compromising their performance, are known problems. Thus, self-tuning vibration neutralisers were introduced to make them more robust. In many cases, however, these systems need an external power source to adapt. This paper concerns an investigation into a self-tuning vibration neutraliser for two distinct frequencies, that does not need an external power source. It consists of a rectangular beam with tip masses, which is held at its centre in a roller bearing that is fixed to a host structure. The rectangular cross section has two different stiffnesses in the local coordinates that can rotate with respect to the global reference. Results from some experimental tests compare very well with time domain numerical simulations. It is shown that the coupling between two orthogonal degrees-of-freedom enables the neutraliser to passively tune to one of two tuned frequencies, depending on the frequency of the external harmonic force.

1. Introduction

Vibration neutralisers and vibration absorbers are devices that may be added to a structure with the aim of reducing or eliminating vibrations at a troublesome resonance or excitation frequency. A vibration absorber is used to reduce vibrations within a certain frequency range around a targeted resonance frequency. The damping can be relatively high to achieve an optimum value to suppress vibration around the resonant frequency. Although very similar to absorbers, neutralisers are devices used to reduce vibrations at a specific frequency, usually caused by an external force. It consists of mass and stiffness elements and is designed with relatively low damping to function as a mechanical notch-filter at a non-resonant frequency and provide the greatest vibration attenuation.

The performance bandwidth of neutralisers is very narrow, and fine tuning of the device is required. If the forcing frequency changes and the natural frequency of the neutraliser no longer matches the forcing frequency, the neutraliser may increase, rather than decrease, the vibration of the host structure. In many practical engineering applications, the frequency of a vibration source is not constant, so a variable stiffness element could be employed to maintain the tuned condition without compromising the neutraliser performance.

Research on self-tuning or self-adaptive vibration neutralisers and absorbers can be found in literature, for example [1,2], and this can be achieved in several ways, for example with

magnetorheological elastomer (MRE) [3–8], with smart materials using shape memory alloy (SMA) [9–15]. Other ways of doing this involve varying the mass moment of inertia [16], and changing the stiffness element geometry [17–19], with rotating spring elements, for example [20–22]. Rasooli et al. [4] presented a semi-active adaptive tuned vibration absorber consisting of a multilayer sandwich beam with MRE layers and electromagnets attached at the top and bottom layers. These provide the magnetic field to alter the MRE stiffness and act as the active mass of the absorber. Sun et al. [5] compared single and multiple layers of MRE on the performance of an adaptive tuned vibration absorber (ATVA). A multilayer MRE absorber was also shown to be effective at attenuating a swept frequency type of vibration over a wide frequency range, and to work at lower frequencies than the single layer MRE absorber. Rustighi et al. [9,10] presented the design and implementation of a ATVA using SMA elements, in which the stiffness and tuned frequency could be continuously adjusted by heating or cooling the SMA. Research on self-adaptive or self-tuning devices are well documented in the literature, however most of these mechanisms rely on an external power source to adapt. This work presents an experimental investigation of a passive self-tuning vibration neutraliser that does not require an external power source to adapt, similar to that proposed by Nehemy et al. [23]. In this paper, a new model for the device is proposed for harmonic force excitation and with an increased number of degrees-of-freedom to capture the base displacement in the time domain simulations. Based on the previous experimental device, a new, improved device has been designed, by changing the geometry and material.

2. Description of the device

2.1. The passive self-tuning vibration neutraliser prototype

The vibration neutraliser prototype consists of an aluminium beam connected to the base through two roller bearings F699-ZZ (inner and outer diameters sizes of 9 and 20mm) one at each side of the base, and is designed to operate in the vertical direction, y_b, of the base coordinate system x_b, y_b, z_b. The total length of the beam is 283 mm. The stiffness element is the rectangular beam that can rotate around the z_b-axis in the bearing, as depicted in Figure 1. Masses of 0.030 kg are attached at each end of the beam. Due to the rectangular cross-section, with dimensions 4.5 by 9 millimetres, two different orthogonal stiffnesses are defined in the tip mass coordinates (x_t, y_t). As the beam rotates around the z_b-axis, the angle θ is defined according to Figure 2, where the position $\theta = 0$ degrees corresponds to when the largest side of the beam cross-section is perpendicular to the excitation force and $\theta = 90$ degrees corresponds when the largest side of the beam cross-section is parallel to the force. The beam, the bearings, and the base together weight 0.129 kg. The tip masses add 0.030 kg at each end, totalling 0.189 kg.

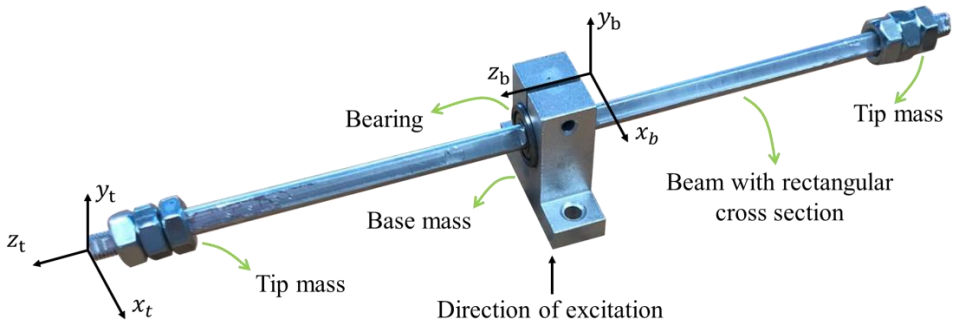

Figure 1. A photograph of the device.

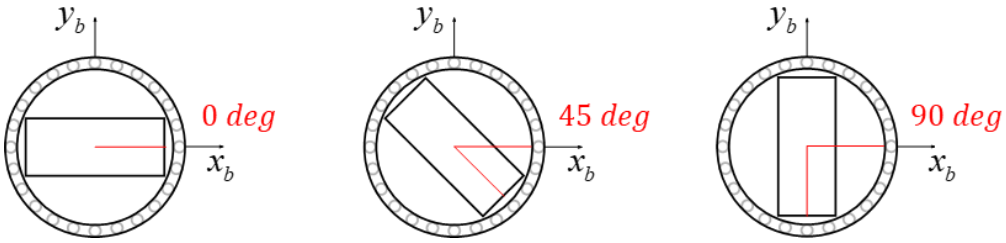

Figure 2. Schematic side view of the neutraliser showing the beam cross section for three angles $\theta = 0$ deg, $\theta = 45$ and $\theta = 90$ deg.

2.2. Lumped parameter frequency domain model – steady-state behaviour

The lumped parameter model shown Figure 3 is developed to obtain physical insight into the steady-state behaviour of the neutraliser when the beam is set at different angles. A simplified linear four degrees-of-freedom model is developed considering the base (x_b, y_b) and tip (x_t, y_t) displacements. This model has free-free boundary conditions and assumes that the angle θ is fixed. It is used to obtain the accelerance transfer functions at fixed angles and the parameters estimated are used later in time-domain simulations of a nonlinear model described in Section 3, in which the beam is free to rotate.

In this linear model the force is applied in the y_b direction on the base mass m_b, which consists of the bearing support block and the outer bearing ring. The tip mass m_t comprises the beam, the masses at the end and the bearing inner ring, and the orthogonal stiffness of the beam in each direction is denoted by k_{yy} and k_{xx} respectively. When $\theta = 0$ degrees, k_{yy} is aligned with the excitation force and the model assumes its lowest orthogonal stiffness in y_b direction. When $\theta = 90$ degrees, k_{xx} is aligned with the excitation force and the model assumes its highest orthogonal stiffness in y_b direction.

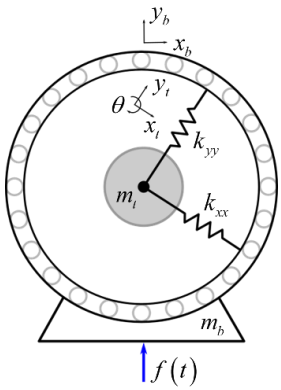

Figure 3. Schematic of the lumped parameter model showing the tip mass and base coordinates.

The lumped parameter frequency domain model can be written down as

$$\mathbf{T}^{\mathrm{T}}(-\omega^2\mathbf{M} + j\omega\mathbf{C} + \mathbf{K})\mathbf{T}\mathbf{q} = \mathbf{f} \tag{1}$$

where $\mathbf{q} = [X_t; Y_t; X_b; Y_b]$ is the displacement vector, $\mathbf{f} = [0; 0; 0; F]$ is the force vector, in which F is the amplitude of the harmonic force applied. The mass and stiffness matrices are $\mathbf{M}$ and $\mathbf{K}$ and are respectively given by

$$\mathbf{M} = \begin{bmatrix} m_t & 0 & 0 & 0 \\ 0 & m_t & 0 & 0 \\ 0 & 0 & m_b & 0 \\ 0 & 0 & 0 & m_b \end{bmatrix}, \mathbf{K} = \begin{bmatrix} k_{xx} & 0 & -k_{xx} & 0 \\ 0 & k_{yy} & 0 & -k_{yy} \\ -k_{xx} & 0 & k_{xx} & 0 \\ 0 & -k_{yy} & 0 & k_{yy} \end{bmatrix} \tag{2}$$

Some viscous damping is also added to the model in a damping matrix $\mathbf{C}$, and a transformation coordinate matrix $\mathbf{T}$ is used to represent the tip mass angular position. These matrices are given by

$$\mathbf{C} = \begin{bmatrix} c_{xx} & 0 & -c_{xx} & 0 \\ 0 & c_{yy} & 0 & -c_{yy} \\ -c_{xx} & 0 & c_{xx} & 0 \\ 0 & -c_{yy} & 0 & c_{yy} \end{bmatrix}, \mathbf{T} = \begin{bmatrix} \cos(\theta) & \sin(\theta) & 0 & 0 \\ -\sin(\theta) & \cos(\theta) & 0 & 0 \\ 0 & 0 & \cos(\theta) & \sin(\theta) \\ 0 & 0 & -\sin(\theta) & -\cos(\theta) \end{bmatrix} \quad (3)$$

Numerical expressions for the resonance and anti-resonance frequencies of the base can be obtained from Equation 1 by inverting the dynamic stiffness matrix analytically and finding the roots of the denominator and numerator for each mode. The resonance frequencies, f_{r1} and f_{r2}, are independent of the angular position of the device and are given by.

$$f_{r1} = \left[\frac{k_{yy}(m_t+m_b)}{m_t m_b}\right]^{1/2} \quad (4)$$

$$f_{r2} = \left[\frac{k_{xx}(m_t+m_b)}{m_t m_b}\right]^{1/2} \quad (5)$$

To compare the model predictions with experimental results, the parameters are estimated through an impact hammer test which is described later. To gain insight into the effect of beam rotation on the system frequency response, an analysis using the analytical expressions for resonances and anti-resonances is conducted with the parameters obtained from the impact hammer tests. Figure 4(a) shows the results of this analysis, with a top view of the frequency response function varying the angle θ from 0 to 90 degrees.

The numerical and experimental frequency response functions are shown in Figure 4 (b-i, b-ii, b-iii) for angles $\theta = 0$, 45 and 90 degrees, respectively. The model and experimental results show good agreement. There are some small differences between the experimental antiresonance frequencies and the model, probably because the model does not consider higher order resonances that are present in the experiment.

It can be seen in Figure 4(a) that when $\theta = 0$ degrees, the anti-resonance frequency f_{a2} and the resonance frequency f_{r2} are the same. This means that there is only one resonance frequency f_{r1} and one anti-resonance frequency f_{a1} in the frequency response, which is shown in Figure 4(b-i). Between 0 and 90 degrees, both resonance frequencies, f_{r1} and f_{r2}, and anti-resonance frequencies, f_{a1} and f_{a2}, are present. Figure 4(b-ii) illustrates the resonances and anti-resonances frequencies in the base accelerance of the particular case $\theta = 45$ degrees. At $\theta = 90$ degrees, Figure 4(a), the anti-resonance frequencies f_{a1} coincides with the resonance frequency f_{r1}, resulting a single resonance frequency f_{r2} and a single antiresonance frequency f_{a2}, which is shown in Figure 4(b-iii).

Simplified expressions can be obtained for the antiresonance frequencies at $\theta = 90$ and $\theta = 0$ to give

$$f_{a1_{90^\circ}} = \left[\frac{k_{yy}m_t + (k_{yy}+k_{xx})m_b - |k_{yy}m_t + (k_{yy}-k_{xx})m_b|}{2m_t m_b}\right]^{1/2} \quad (6)$$

$$f_{a2_{0^\circ}} = \left[\frac{k_{xx}m_t + (k_{yy}+k_{xx})m_b + |k_{xx}m_t + (k_{xx}-k_{yy})m_b|}{2m_t m_b}\right]^{1/2} \quad (7)$$

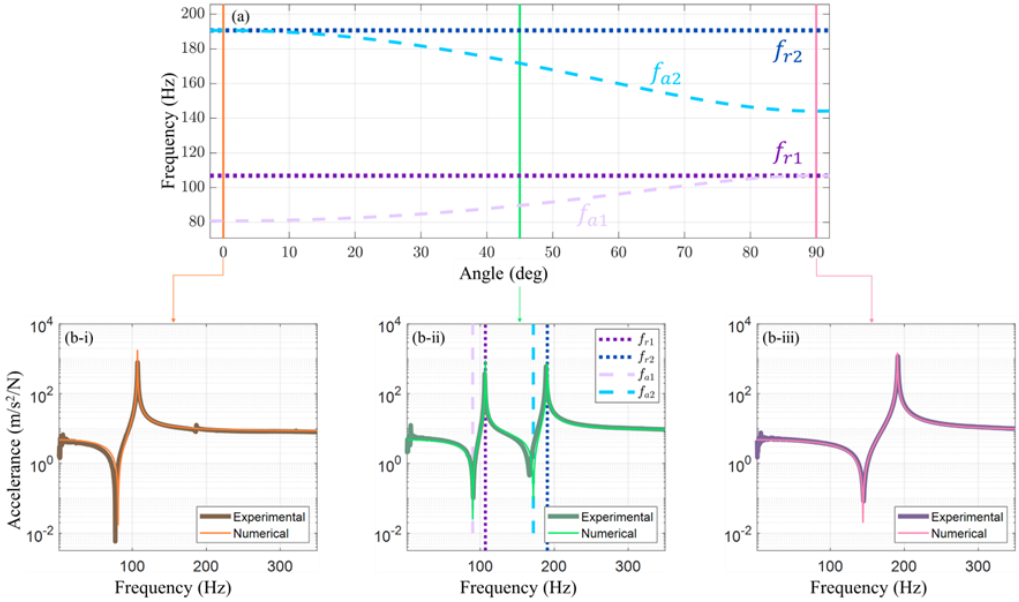

Figure 4. Effect of the spin angle θ on the frequency response functions. Subfigure (a) shows the resonance and anti-resonance behaviour as a function of θ; (b) compares the experimental and numerical results at different angles (i) $\theta = 0$, (ii) $\theta = 45$ and (iii) $\theta = 90$ degrees.

The parameters of the neutraliser were determined through impact hammer experiments with the device at three angles $\theta = 0$, $\theta = 45$ and $\theta = 90$ degrees. The neutraliser was suspended by wires and the base was excited using a modal hammer PCB-086C01 with a medium stiffness tip. The responses were measured at three points, one in the base and two on the tip mass, using PCB-352A24 accelerometers. The signals were recorded using a SIRIUSm-4xACC acquisition system with a sampling frequency of 1 kHz. The transfer accelerances (acceleration/force) were estimated using the H_1 transfer function estimator in dedicated software of the acquisition system, and four averages were taken. The parameters of the model were determined qualitatively by setting low and high frequencies asymptotes and matching the resonance frequencies. The resulting parameters, displayed in Table 1, were subsequently used in time and frequency-domain simulations.

Table 1. Parameters estimated from the impact hammer tests.

Property	
Base mass (m_b)	0.120 kg
Tip mass (m_t)	0.090 kg
Stiffness in x direction (k_{xx})	73800 N/m
Stiffness in y direction (k_{yy})	23200 N/m
Viscous damping in x direction (c_{xx})	0.15 Ns/m
Viscous damping in y direction (c_{yy})	0.07 Ns/m
f_{r1}	107 Hz
f_{r2}	191 Hz
f_{a1} at $\theta = 90$ degrees	107 Hz
f_{a2} at $\theta = 0$ degrees	191 Hz

3. Time domain model of the neutraliser

Having validated the frequency domain model of the neutraliser a time domain model is developed to simulate the behaviour of the vibration neutraliser when subjected to harmonic excitation. A five degrees-of-freedom lumped parameter model is developed considering the base displacements (x_b, y_b), the tip displacements (x_t, y_t) and the rotation around the z_b-axis, described by θ. In this model, the elastic forces depend on the angular orientation of the device and hence are functions of time. The equations of motion are obtained by applying Lagrange's method. The kinetic energy involves the base and tip masses and the inertia due to the tip mass rotation. The potential energy is a result of the strain energy stored in the springs and the gravitational field. A Rayleigh term is added to include viscous damping. Considering, $\tilde{c} = (c_{yy} - c_{xx})$, $\tilde{k} = (k_{yy} - k_{xx})$, $\dot{z}_y = (\dot{y}_b - \dot{y}_t)$, $z_y = (y_b - y_t)$, $\dot{z}_x = (\dot{x}_b - \dot{x}_t)$, $z_x = (x_b - x_t)$ and $f(t) = F\cos(\omega t)$ is the harmonic force applied in the y_b direction, the equations of motion are found to be

$$I\ddot{\theta} + c_t\dot{\theta} - \tilde{k}\left[z_x z_y \cos(2\theta) + \frac{1}{2}\left({z_y}^2 - {z_x}^2\right)\sin(2\theta)\right] = 0 \tag{8}$$

$$m_t\ddot{x}_t + \frac{1}{2}\left[\left(\tilde{c}\dot{z}_y + \tilde{k}z_y\right)\sin(2\theta) - \left(\tilde{c}\dot{z}_x - \tilde{k}z_x\right)\cos(2\theta) + \tilde{c}\dot{z}_x + \tilde{k}z_x\right] - k_{yy}z_x = 0 \tag{9}$$

$$\begin{aligned} m_t\ddot{y}_t + \frac{1}{2}\left[\left(\tilde{c}\dot{z}_x + \tilde{k}z_x\right)\sin(2\theta) - \left(\tilde{c}\dot{z}_y + \tilde{k}z_y\right)\cos(2\theta) - \tilde{c}\dot{z}_y - \tilde{k}z_y\right] - c_{xx}\dot{z}_y \\ - k_{xx}z_y \ + gm_t = 0 \end{aligned} \tag{10}$$

$$\begin{aligned} m_b\ddot{x}_b - \frac{1}{2}\left[\left(\tilde{c}\dot{z}_y + \tilde{k}z_y\right)\sin(2\theta) + \left(\tilde{c}\dot{z}_x + \tilde{k}z_x\right)\cos(2\theta) + \tilde{c}\dot{z}_x + \tilde{k}z_x\right] + c_{yy}\dot{z}_x \\ + k_{yy}z_x = 0 \end{aligned} \tag{11}$$

$$\begin{aligned} m_b\ddot{y}_b - \frac{1}{2}\left[\left(\tilde{c}\dot{z}_x + \tilde{k}z_x\right)\sin(2\theta) - \left(\tilde{c}\dot{z}_y + \tilde{k}z_y\right)\cos(2\theta) \ - \ \tilde{c}\dot{z}_y - \tilde{k}z_y\right] + c_{xx}\dot{z}_y \\ + k_{xx}z_y + gm_b = f(t) \end{aligned} \tag{12}$$

The equations of motion are solved by numerical integration using the Runge-Kutta method. To identify the behaviour of the neutralizer as the angle of rotation is changed, the harmonic forcing frequency is varied. The amplitude of the force is kept constant at $F = 5$ N, and the excitation frequency is varied from 1 to 350 Hz. The initial conditions for each frequency are $\theta_0 = 45$ degrees and with zero displacements and velocities. At the end of a time period when the response is in steady-state, the angle θ is noted. The results are depicted in Figure 5(a), in which the black line is the final angle for the frequency range analyzed. Also shown are the resonances frequencies f_{r1} and f_{r2}. It can be seen that these frequencies are important in influencing the final angle to which the device settles. If the excitation frequency is below the first resonance frequency f_{r1}, the neutraliser tunes to 0 degrees. If the frequency is between the two resonance frequencies f_{r1} and f_{r2}, the neutraliser tunes to 90 degrees, and above the second resonance frequency f_{r2} the neutraliser tunes to 0 degrees.

To gain insight into this behaviour, the predicted amplitude of the device at 0 and at 90 degrees is plotted in Figure 5(b) using the frequency domain model. The thick lines show the amplitudes of the accelerance for the tuning angle at each frequency. The dot-dashed red lines, indicated by (i), (ii) and (iii) are the frequencies at which subsequent numerical and experimental studies are carried out, which are described in the next section. These frequencies are 70, 140 and 170 Hz. It is expected that the device will tune to $\theta = 0$ degrees when excited with 70 Hz and $\theta = 90$ degrees when excited with 140 and 170 Hz.

The vibration neutralizer proposed in this study outperforms conventional neutralizers with low damping. This is attributed to its effectiveness in two frequency ranges, due to the presence of two antiresonances. By switching the angle to 0 or 90 degrees, the device adapts to one or the other antiresonance frequency, based on the excitation frequency. Conventional neutralizers, with only one antiresonance frequency, have a narrow bandwidth around the antiresonance frequency, which limits their tuning capabilities.

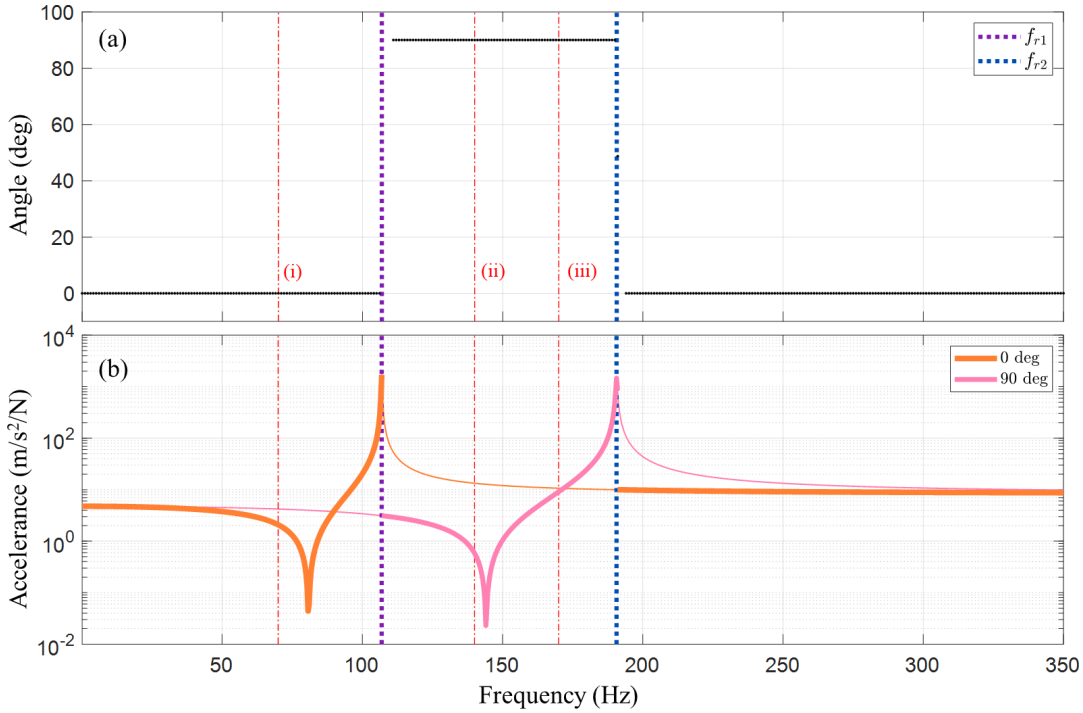

Figure 5. Correlation between the harmonic excitation frequency, the tuning angle and the base accelerance. Subfigure (a) indicates a numerical time-domain analysis varying the excitation frequency and (b) displays the base accelerance at 0 and 90 degrees. The dot-dashed red lines indicate (i) 70, (ii) 140 and (iii) 170 Hz.

4. Self-tuning experimental and numerical investigation with harmonic excitation

The experimental rig is shown in Figure 6. The neutraliser was fixed to an LDS V406 electrodynamic shaker through a DYTRAN 1051V2 force sensor. The base acceleration a_{y_b} was measured using a PCB-352A24 accelerometer and was recorded using a SIRIUSm-4xACC data acquisition system (not shown in the figure) with a sampling frequency of 2 kHz. To mitigate the potential interference caused by an accelerometer on the beam rotation, the angular displacement of the beam θ was recorded utilizing a Basler Ace 2 Camera – a2A1920-160umBAS with Basler Lens C23-1620-5M-P f16mm operating at 720 frames per second (not shown in the figure). The time history for the angular displacement of the beam was extracted from the recorded movie using the Tracker Physics software [24].

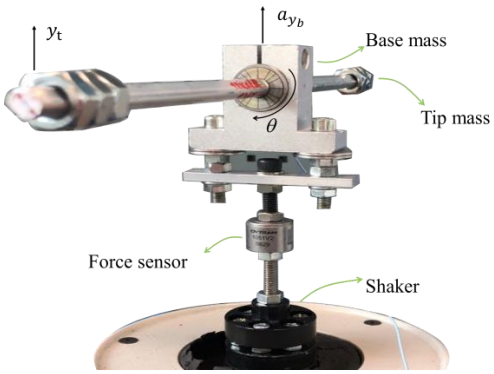

Figure 6. Experimental rig showing the shaker and the force sensor and the device.

The experimental results, shown in Figure 7, are compared with the numerical results, shown in Figure 8. The excitation frequencies were 70 Hz (subfigure (a)), 140 Hz (subfigure (b)) and 170 Hz (subfigure (c)). Subfigures (i) display the angle in degrees and subfigures (ii) display the base acceleration in m/s^2. The experimental and numerical results show a strong agreement in the time needed to tune the device, the behaviour and levels of the base acceleration. Additionally, the expected tuning angle, obtained numerically for each frequency, matches well with the experimental results. The experimental and numerical results exhibit slight variations in their time responses. However, these differences have been mitigated through the process of manual optimization of the torsional and viscous damping coefficients and excitation force amplitude. These parameters were adopted in the numerical model to yield a similar tuning response of the neutraliser, with equivalent tuning time and overshoot.

At the excitation frequencies of 70 Hz and 140 Hz, shown in Figure 7(a) and Figure 7(b) respectively, the base acceleration decreases after the tuning and the device perform as a vibration neutraliser. For an harmonic base excitation at 170 Hz, shown in Figure 7(c), the device does not perform as a vibration neutraliser since the base acceleration frequency does not match one of the two anti-resonances (tuning frequencies). This performance prediction is also shown in Figure 5(b), which was obtained with the numerical model.

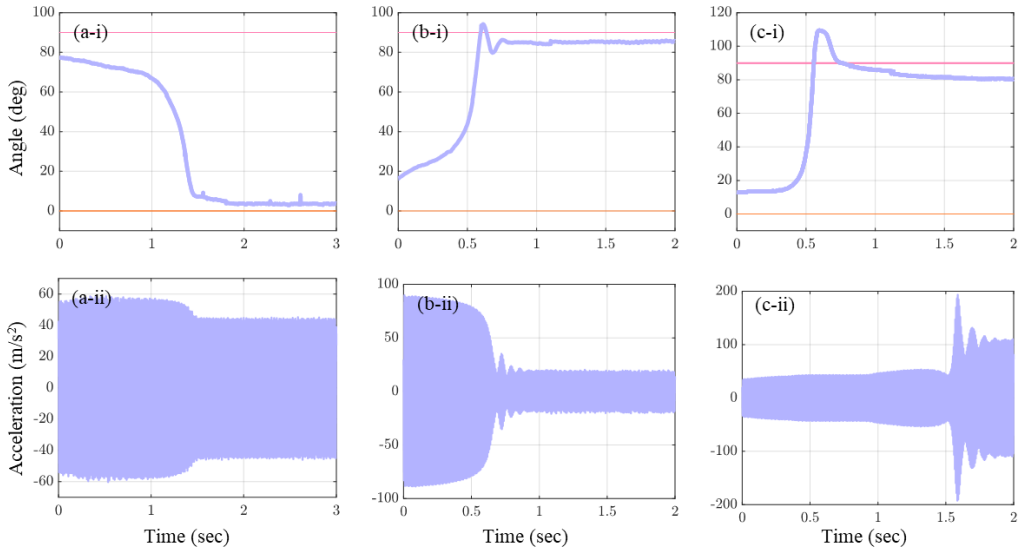

Figure 7. Experimental time stories for (a) angle and (b) base acceleration. Subfigures shows different excitation frequency (i) 70 Hz, (ii) 140 Hz and (iii) 170 Hz.

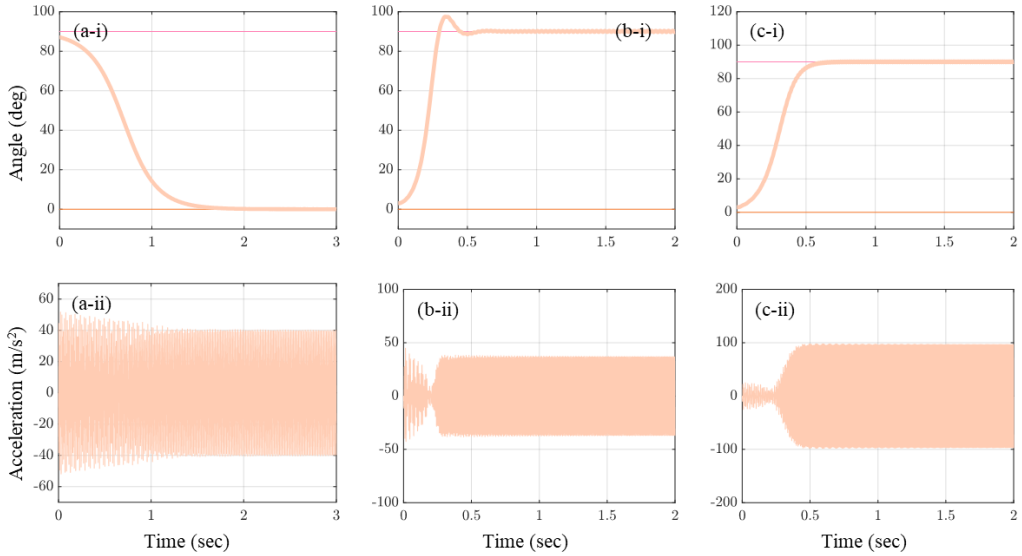

Figure 8. Numerical time stories for (a) angle and (b) base acceleration. Subfigures shows different excitation frequency (i) 70 Hz, (ii) 140 Hz and (iii) 170 Hz.

5. Conclusions

This work has presented a theoretical and experimental investigation of a passive self-tuning vibration neutraliser that does not require an external power source to adapt. The intended use for the vibration neutraliser is to self-tune when subject to an excitation force reducing the host structure vibration at a harmonic forcing frequency. Since the device has two anti-resonance frequencies, it may be effective at two harmonic excitation frequencies. A Simple model has been developed to gain some physical insight into the behaviour of the device in both the time and frequency domains. The experimental results and model output showed good agreement. The vibration neutraliser can passively tune to either one of its two tuning conditions, depending on the harmonic forcing frequency, increasing the performance bandwidth. If this excitation frequency is below the lowest resonant frequency of the device the neutraliser tunes to 0 degrees. If the excitation frequency is between the two resonant frequencies of the device the neutraliser tunes to 90 degrees. When the excitation frequency is above the highest resonant frequency, the neutraliser tunes to 0 degrees. Additional analyses are currently being undertaken with different devices in order to investigate the effect of the mass and stiffness ratios on the anti-resonances behaviour and on the frequency regions where base attenuation occurs.

6. Acknowledgments

We gratefully acknowledge support of CNPq – National Council for Scientific and Technological Development (Grant Number 406594/2021-0), FAPESP – São Paulo Research Foundation (Grant Numbers 2018/15894-0 and 2020/00534-9) and CAPES – National Council for the Improvement of Higher Education (Grant Numbers 88887.513387/2020-00 and 88881.690385/2022-01).

References

[1] Sun J Q, Jolly I R and Norris M A 1995 *Passive, Adaptive and Active Tuned Vibration Absorbers-A Survey*

[2] Brennan M J 2006 *Some recent developments in adaptive tuned vibration absorbers/neutralisers* vol 13 (IOS Press)

[3] Khanouki M A, Sedaghati R and Hemmatian M 2020 Multidisciplinary design optimization of a novel sandwich beam-based adaptive tuned vibration absorber featuring magnetorheological elastomer *Materials* **13**

[4] Rasooli A, Sedaghati R and Hemmatian M 2020 A novel magnetorheological elastomer-based adaptive tuned vibration absorber: Design, analysis and experimental characterization *Smart Mater Struct* **29**
[5] Sun S, Deng H, Yang J, Li W, Du H, Alici G and Nakano M 2015 An adaptive tuned vibration absorber based on multilayered MR elastomers *Smart Mater Struct* **24**
[6] Sun S S, Chen Y, Yang J, Tian T F, Deng H X, Li W H, Du H and Alici G 2014 The development of an adaptive tuned magnetorheological elastomer absorber working in squeeze mode *Smart Mater Struct* **23**
[7] Deng H X and Gong X L 2007 Adaptive tuned vibration absorber based on magnetorheological elastomer *Journal of Intelligent Material Systems and Structures* vol 18 pp 1205–10
[8] Deng H X, Gong X L and Wang L H 2006 Development of an adaptive tuned vibration absorber with magnetorheological elastomer *Smart Mater Struct* **15**
[9] Rustighi E, Brennan M J and Mace B R 2005 Real-time control of a shape memory alloy adaptive tuned vibration absorber *Smart Mater Struct* **14** 1184–95
[10] Rustighi E, Brennan M J and Mace B R 2005 A shape memory alloy adaptive tuned vibration absorber: Design and implementation *Smart Mater Struct* **14** 19–28
[11] Liao Y T, Lin J H and Lee C Y 2018 A tuned vibration absorber constituted of shape memory alloy wires for vibration reduction of platform structures: Design and implementation *MATEC Web of Conferences* vol 185 (EDP Sciences)
[12] Huang H, Chang W S and Mosalam K M 2017 Feasibility of shape memory alloy in a tuneable mass damper to reduce excessive in-service vibration *Struct Control Health Monit* **24**
[13] Berardengo M, Cigada A, Guanziroli F and Manzoni S 2015 Modelling and control of an adaptive tuned mass damper based on shape memory alloys and eddy currents *J Sound Vib* **349** 18–38
[14] Williams K A, Chiu G T C and Bernhard R J 2005 Dynamic modelling of a shape memory alloy adaptive tuned vibration absorber *J Sound Vib* **280** 211–34
[15] Williams K A, Chiu G T C and Bernhard R J 2005 Nonlinear control of a shape memory alloy adaptive tuned vibration absorber *J Sound Vib* **288** 1131–55
[16] Shakib A and Ghorbani-Tanha A K 2020 An innovative adaptive tuned vibration absorber with variable mass moment of inertia for mitigation of transient response of systems *Struct Control Health Monit* **27**
[17] Brennan M J 1998 Actuators for active vibration control-tunable resonant devices *Proceedings of the 4th European Conference on Smart Materials and Structures* pp 41–8
[18] Bonello P, Brennan M J and Elliott S J 2005 Vibration control using an adaptive tuned vibration absorber with a variable curvature stiffness element *Smart Materials and Structures* vol 14 pp 1055–65
[19] Nagaya K, Kurusu A, Ikai S and Shitani Y 1999 Vibration control of a structure by using a tunable absorber and an optimal vibration absorber under auto-tuning control *J Sound Vib* **228** 773–92
[20] Rustighi E 2010 A tunable vibration absorber based on rotating stiffness elements (University of Southampton)
[21] Varadarajan N, Nagarajaiah S and Asce M Wind Response Control of Building with Variable StiffnessTuned Mass Damper Using Empirical Mode Decomposition/Hilbert Transform
[22] Carneal J P, Charette F and Fuller C R 2004 Minimization of sound radiation from plates using adaptive tuned vibration absorbers *J Sound Vib* **270** 781–92
[23] Nehemy G F, Rustighi E, Gonçalves P J P and Brennan M J 2023 A passive self-tuning vibration neutraliser using nonlinear coupling between the degrees of freedom *Mech Syst Signal Process* **185** 109786
[24] Brown D, Hanson R and Christian W 2023 Tracker Video Analysis and Modeling Tool *https://physlets.org/tracker/*